Chinese Journal of Natural Medicines

Combining label-free quantitative proteomics and 2D-DIGE to identify the potential targets of Sini Decoction acting on myocardial infarction

Fei Feng, Weiyue Zhang, Yan Cao, Diya Lv, Yifeng Chai, Dandan Guo, Xiaofei Chen

Citation: Fei Feng, Weiyue Zhang, Yan Cao, Diya Lv, Yifeng Chai, Dandan Guo, Xiaofei Chen, Combining label-free quantitative proteomics and 2D-DIGE to identify the potential targets of Sini Decoction acting on myocardial infarction, Chinese Journal of Natural Medicines, 2025, 23(8), 1016-1024. doi: 10.1016/S1875-5364(25)60937-X.

View online: https://doi.org/10.1016/S1875-5364(25)60937-X

Chinese Journal of Natural Medicines 23 (2025) 1016-1024

Contents lists available at ScienceDirect

Chinese Journal of Natural Medicines

journal homepage: www.cjnmcpu.com/

Original article

Combining label-free quantitative proteomics and 2D-DIGE to identify the potential targets of Sini Decoction acting on myocardial infarction

Fei Feng[a,b,c,Δ], Weiyue Zhang[d,Δ], Yan Cao[a], Diya Lv[a,b], Yifeng Chai[a,b,*], Dandan Guo[a,b,*], Xiaofei Chen[a,b,*]

[a] School of Pharmacy, Naval Medical University (Second Military Medical University), Shanghai 200433, China
[b] Shanghai Key Laboratory for Pharmaceutical Metabolite Research, Shanghai 200433, China
[c] Department of Pharmacy, Shanghai Changhai Hospital, Naval Medical University (Second Military Medical University), Shanghai 200433, China
[d] School of Nursing, Beijing University of Chinese Medicine, Beijing 102488, China

ARTICLE INFO

Article history:
Received 10 September 2024
Revised 13 December 2024
Accepted 24 February 2025
Available online 20 August 2025

Keywords:
Sini Decoction
Myocardial infarction
Drug affinity response target stability
Label-free quantitative proteomics

ABSTRACT

Sini Decoction (SNT) is a traditional formula recognized for its efficacy in warming the spleen and stomach and dispersing cold. However, elucidating the mechanism of action of SNT remains challenging due to its complex multiple components. This study utilized a synergistic approach combining two-dimensional fluorescence difference in gel electrophoresis (2D-DIGE)-based drug affinity responsive target stability (DARTS) with label-free quantitative proteomics techniques to identify the direct and indirect protein targets of SNT in myocardial infarction. The analysis identified 590 proteins, with 30 proteins showing significant upregulation and 51 proteins showing downregulation when comparing the SNT group with the model group. Through the integration of 2D-DIGE DARTS with proteomics data and pharmacological assessments, the findings indicate that protein disulfide-isomerase A3 (PDIA3) may serve as a potential protein target through which SNT provides protective effects on myocardial cells during myocardial infarction.

1. Introduction

Sini Decoction (SNT) is a classic traditional Chinese medicine prescription comprising Aconiti Lateralis Radix Praeparata (Fuzi), Glycyrrhizae Radix et Rhizome Praeparata cum Melle (Zhigancao), and Zingiberis Rhizoma (Ganjiang). In Chinese clinical practice, SNT demonstrates effectiveness in treating cardiovascular diseases, including shock, acute and chronic myocardial infarction, and heart failure [1-6]. Studies indicate that aconitine alkaloids in Aconiti Lateralis Radix Praeparata and flavonoid components in Glycyrrhizae Radix et Rhizome Praeparata cum Melle interact with adrenaline receptors, ion channel proteins, and other myocardial cell membrane receptors. Liquiritin and 6-gingerol enhance aconitine absorption and increase its blood concentration by inhibiting P-glycoprotein activity [7]. The combination of songorine, 8-gingerol, and isoliquiritigenin from SNT shows promise as a prebiotic agent in mitigating doxorubicin-induced cardiomyopathy through modulation of mitochondrial energy metabolism and dysfunction [8].

Our research group has previously conducted a comprehensive analysis of SNT's chemical composition, identifying 53 main components in serum [9]. We analyzed membrane receptor affinity fractions in aconite using full two-dimensional comparative cardiomyocyte membrane chromatography, characterizing 16 aconitine alkaloids [10-12]. Furthermore, our research confirmed talatizamine's apoptosis-protective activity in cardiomyocytes [13]. Although the active constituents and clinical applications of SNT have been extensively studied, current methodologies cannot comprehensively characterize SNT's protein targets or definitively identify and validate targets *in vivo* [14]. Thus, developing novel approaches for target analysis of SNT is crucial.

Drug affinity responsive target stability (DARTS) represents a negative enrichment method where drug binding enhances target protein stability, making them resistant to protease digestion [15, 16]. DARTS technology's primary advantage lies in its use of unmodified small molecules, making it particularly suitable for target screening in complex Chinese medicine systems [17].

To identify potential direct or indirect targets of SNT's myocardial action, this study first investigated protein biomarkers using state-of-the-art label-free quantitative proteomics technology. Subsequently, utilizing the DARTS technique coupled with two-dimensional fluorescence difference gel electrophoresis (2D-DIGE), the study identified direct targets of SNT's action on H9c2 cardiomyocytes. Fig. 1 illustrates the comprehensive workflow. This investigation aims to elucidate SNT's possible *in vivo* targets and mechanism of action, providing a fundamental framework for target discovery in traditional Chinese medicine systems.

2. Materials and methods

2.1. Reagents and materials

Aconiti Lateralis Radix Praeparata (Fuzi), Glycyrrhizae Radix

* Corresponding author.
E-mail addresses: yfchai@smmu.edu.cn (Y. Chai); dana_guo0826@163.com (D. Guo); xfchen2010@163.com (X. Chen)
Δ These authors contributed equally to this work.

https://doi.org/10.1016/S1875-5364(25)60937-X

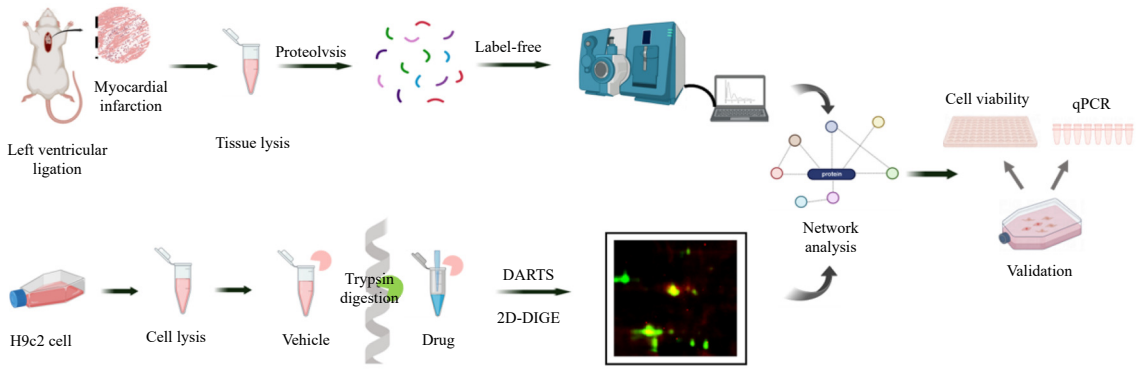

Fig. 1 The schematic illustration of the study.

et Rhizome Praeparata cum Melle (Zhigancao), and Zingiberis Rhizoma (Ganjiang) were obtained from Shanghai Lei Yunshang Pharmaceutical Co., Ltd. (Shanghai, China), and identified by Prof. Chengzhong Zhang (Naval Medical University). SNT was prepared in accordance with the 2020 edition of *Chinese Pharmacopoeia* Part I. Sprague-Dawley (SD) rats were acquired from Shanghai SLAC Laboratory Animal Co., Ltd. (Shanghai, China) and maintained under controlled environmental conditions at temperatures between 20 to 25 °C and humidity between 50% and 60%. All animal experiments were performed in strict compliance with applicable international regulations and regional guidelines.

2.2. Experimental models of myocardial infarction mice

30 SD rats (180–220g) underwent surgical procedures, yielding 11 survivors in the sham group and 17 in the model group. The latter were subsequently divided randomly into two subgroups: 8 in the infarction model group and 9 in the SNT group. The SNT group received 10 g·kg^{-1} BW of SNT extract, equivalent to the original medicinal material, while an identical volume of physiological saline was administered to both the model and sham groups. This treatment protocol continued once daily for 14 consecutive days following model induction. The experiments received approval from the Ethics Review of Lab Animal Use Application of Naval Medical University.

The rat model of myocardial infarction was established in SD male rats through surgical ligation of the left anterior descending (LAD) coronary artery. The procedure was performed as follows: rats were anesthetized with ether, and the left atrial appendage was carefully lifted using ophthalmic forceps. The LAD coronary artery was ligated using a 5/0 surgical suture approximately 1 mm below the aortic cone and left atrial appendage. For the sham group, the procedure remained identical, except suture loops were placed without ligation.

The Visual Sonics Vevo 770 micro-ultrasound imaging system (Visual Sonic Inc., Canada) was employed for echocardiographic assessments. The probe recorded the average values of 5 cardiac cycles while simultaneously capturing and storing images and videos. The M-mode was utilized to analyze essential cardiac functional indicators, including ejection fraction (EF).

2.3. Immunohistochemical detection

Rat left ventricular tissues underwent dewaxing and rehydration, followed by anti-genic repair and overnight incubation with fibrinogen α (FIB α, 1∶1600), heat shock protein 90 α/β (HSP90 α/β, 1∶800), protein disulfide-isomerase A3 (PDIA3, 1∶800) and gap junction alpha-1 protein (CX43, 1∶800) primary antibodies, respectively, followed by incubation with rabbit secondary antibody at 37 °C for 1 h. Freshly prepared DAB was applied dropwise to each slide, which was then incubated with rabbit secondary antibody for 2 h at 37 °C. The nuclei were subsequently stained with hematoxylin, differentiated using hydrochloric acid alcohol, and briefly exposed to the blue solution, after which nuclear coloration was examined under the microscope. The tissue slides were then dried in anhydrous alcohol and photographed under a white light microscope.

2.4. Serum biochemical analysis

Serum samples were collected and analyzed at the Testing & Analysis Centre (Naval Medical University). Lactate dehydrogenase (LDH), alanine aminotransferase (ALT), and aspartate aminotransferase (AST) were measured using a biochemistry analyser (Hitachi 7180, Tokyo, Japan) to assess cardiac function index.

2.5. Protein extraction and enzymatic digestion

Rat left ventricular tissue samples were minced with scissors and washed 3 times with 1 × phosphate-buffered saline (PBS) buffer. Excess moisture was removed from the samples using filter paper. Following the addition of lysis buffer, low-temperature grinding was conducted using a tissue homogenizer. The samples were then lysed on ice for 45 min, centrifuged at 15 000 r·min^{-1} for 15 min at 4 °C, and the supernatant was collected. Protein concentration was determined precisely using the bicinchoninic acid (BCA) method. Protein samples were incubated with 10 mmol·L^{-1} dithiothreitol at 37 °C for 1 h and 55 mmol·L^{-1} iodoacetamide at room temperature for 45 min in darkness. Five times the volume of pre-cooled acetone was added to the sample for overnight precipitation at −20 °C. The samples were centrifuged at 4 °C for 10 min at 14 000 r·min^{-1}.

Resuspend the protein precipitate in a 50 mmol·L^{-1} ammonium bicarbonate solution, and add trypsin (enzyme/protein = 1∶50) to the samples for incubation at 37 °C for 16 h. Following digestion, the samples were stored at −80 °C overnight and subsequently desalted using Pierce C_{18} Spin columns according to the manufacturer's protocol. The samples were then dried in a vacuum concentrator.

2.6. H9c2 cell culture

Rat H9c2 cells were obtained from the American Model Culture Collection (Maryland, USA) and maintained in Dulbecco's Modified Eagle's Medium supplemented with 10% fetal bovine serum, streptomycin, and penicillin at 37 °C with 5% CO_2 in a 95% humidified atmosphere.

2.7. Western blotting

Proteins were extracted with RIPA buffer containing protease inhibitor cocktail, separated on SDS-PAGE gel, and electro-

transferred to PVDF membranes. The samples were incubated with appropriate primary (Proteintech, China) and secondary antibodies (LI-COR, Inc). The protein bands were visualized using the Oddysey Fc detection system (LI-COR, Inc.).

2.8. DARTS experiment

H9c2 cells were collected and washed with ice-cold PBS when they reached approximately 80%–85% confluence. Cell lysis buffer was added and cells were lysed on ice for 30 min, then centrifuged at 4 °C to collect the supernatant. Subsequently, the BCA assay determined the protein concentration [13]. 500 μg protein was prepared for control and SNT groups, respectively. The samples were then parallelly incubated with proteins for 60 min at room temperature with moderate shaking. Finally, a final concentration of 0.6% pronase was added to the sample for 30 min at 25 °C.

2.9. Difference gel electrophoresis (DIGE) experiment

The protein samples were fluorescently labeled using the DIGE minimal labeling kit (GE, USA). Following purification, the protein samples were lysed with 50 μL of lysis buffer in the dark. One group of samples was labeled with cy2 without the pronase enzyme, while another group along with the enzyme and SNT sample was labeled with cy3. A third group with enzyme was labeled, excluding SNT. Subsequently, the labeled samples were mixed and incubated at 4 °C for 30 min. To halt the reaction, 1 μL of 10 mmol·L^{-1} lysine was added and mixed, allowing for a 10-min termination period. To initiate further processing, an equal volume of 2 × loading buffer solution [7 mol·L^{-1} urea, 2 mol·L^{-1} thiourea, 4% CHAPS, 100 mmol·L^{-1} DTT, and 1% (*W*/*V*) IPG ampholytes at pH 3–10] was added separately to each sample. Following mixing and supplementation with 1 × loading buffer to reach a final volume of 300 μL, the samples were prepared. Subsequently, 17 cm pH 3–10 NL IPG preformed gel strips (Bio-Rad, USA) were applied to initiate isoelectric focusing and bi-directional electrophoresis analysis. DIGE-Typhoon variable mode image scanner (Amasya, Sweden) was utilized to visualize the Cy-Dye labeled proteins. Ettan DIGE software was employed for the analysis of DIGE images, enabling the identification of significant variations.

2.10. In-gel digestion

The gel was rinsed twice with ultrapure water. Decolorization solution (30 mmol·L^{-1} potassium ferricyanide and 100 mmol·L^{-1} sodium thiosulphate mixed in equal volume) was added and maintained for 2 min until colorless. The coomassie-stained gel was destained by adding 100 μL of 100 mmol·L^{-1} ammonium bicarbonate/acetonitrile solution (1∶1) and incubated at room temperature for 30 min. Subsequently, 100 μL of acetonitrile was added, and the gel was incubated for 10 min to dehydrate and shrink. Trypsin was added to the gel and incubated at 37 °C overnight in a thermomixer. The following day, the supernatant was collected, and extraction solution (2.5% TFA and ACN in equal volumes) was added to the gel, sonicated for 1 min, and then maintained at 37 °C for 60 min. Acetonitrile was added to the gel for 60 min at room temperature. The supernatants were collected and dried in a vacuum centrifuge.

2.11. Nano-liquid chromatography linear ion trap quadrupole Orbitrap mass spectrometry (NanoLC-LTQ-Orbitrap-MS) analysis

Peptides were analyzed using a nano-liquid chromatography system coupled to an LTQ-Orbitrap mass spectrometer (Thermo Fisher Scientific, USA). Separation was performed on an UltiMate 3000 RSLCnano system equipped with an Acclaim PepMap RSLC C_{18} (2 μm, 100 Å, 75 μm i.d. × 50 cm). The mobile phases consisted of solvent A (0.1% formic acid in water) and solvent B (80% acetonitrile with 0.1% formic acid). Chromatographic separation was achieved at a constant flow rate of 350 nL·min^{-1} using the following gradient program: 5% B (initial), increased to 25% B over 20 min, then to 35% B over 90 min, followed by 50% B over 40 min, ramped to 80% B over 20 min, returned to 5% B within 1 min, and maintained at 5% B for 19 min to re-equilibrate the column. Mass spectrometry was conducted in positive ion mode using the Orbitrap for full MS scans (*m/z* 300–2000) at a resolution of 30 000. Data-dependent acquisition was employed to fragment the top 10 most intense precursor ions using collision-induced dissociation in the linear ion trap. The ion accumulation threshold for MS/MS was set at 500 counts, with a normalized collision energy of 35%, an activation *Q*-value of 0.25, and an activation time of 10 ms. Dynamic exclusion was enabled with a repeat duration of 30 s to minimize redundant fragmentation. Nanospray ionization was performed using a spray voltage adjusted between 1.7 and 2.1 kV, optimized according to spray stability. No sheath gas was applied during ionization. Data acquisition and instrument control were managed using Thermo Xcalibur software.

2.12. Data analysis

Data analysis was performed using MaxQuant 2.0.1.0. RAW files were exported, and the experimental design was configured to search the rat protein sequence database (Rat_organism_uniprot, Swiss-Prot/TrEMBL: http://www.expasy.org). The search parameters were precisely defined: mass tolerance was set to 20; trypsin was used for enzyme digestion; up to 1 maximum missed cleavage was permitted; variable modifications included methionine oxidation and protein *N*-acetylation; cysteine alkylation was specified as a fixed modification; the FDR value was maintained at 1%; label-free quantification was employed, with a peak alignment parameter (match between runs) of 2 min, while other parameters remained at default settings.

2.13. Cell viability

Cells were seeded in a 96-well plate at a density of 1 × 10^4 cells/well overnight, then incubated with varying concentrations of SNT for 2 h. 2 μmol·L^{-1} hydrochloride doxorubicin (DOX, TargetMOI, China) was added to the cells to induce the myocardial injury model. Cell viability was measured using the cell counting kit-8 (CCK-8) kit according to the manufacturer's instructions.

2.14. Reverse transcription-quantitative polymerase chain reaction (RT-qPCR)

Total ribonucleic acid (RNA) was extracted from cells using an RNA extraction kit according to the protocol. First-strand complementary deoxyribonucleic acid (cDNA) was synthesized from 500 ng total RNA using Prime Script Strand cDNA Synthesis Kit (TaKaRa, Japan). RT-qPCR was conducted on a real-time thermal cycler (Jielaimei, China) with three biological replicates using Bestar® SybGreen qPCR Mastermix (DBI Bioscience, Germany). *Gapdh* served as an internal control. The primers used are available at https://www.sangon.com/.

2.15. Molecular docking

The PDIA3 (PDB ID: 7QNG) was obtained from the Protein Data Bank (PDB), while higenamine hydrochloride (Hig) and mesaconitine (Mes) were obtained from the PubChem database (https://pubchem.ncbi.nlm.nih.gov/). AutoDock Vena was util-

ized for the hydrogenation and dehydration processes. Molecular docking and visualization were subsequently performed using PyMOL.

3. Results

3.1. The effect of SNT on heart function

As illustrated in Fig. 1, the study was designed to investigate the potential targets of SNT in treating myocardial infarction. The rat model of myocardial infarction was established by ligating the LAD branch of the coronary artery. To evaluate the therapeutic effect of SNT on myocardial infarction, echocardiography was performed using an echocardiography analyzer to observe the effects of modeling and drugs on cardiac function. Left ventricular EF represents a crucial indicator of cardiac function. EF% = [(LVEDV − LVESV)/LVEDV] × 100. LVEDV: left ventricular end-diastolic volume; LVESV: left ventricular end-systolic volume.

The representative echocardiographic results from the Sham, Model, and SNT group are presented in Fig. 2A. Based on EF%, FS%, and LVEDV index, the left ventricular wall fibrillation in the model group was eliminated, confirming successful model establishment. Following continuous gastric administration over 14 d, the SNT group demonstrated significant improvement in EF% (46.04%) compared to the model group (24.98%) (Fig. 2B), consistent with previous research findings [18]. The histopathological examination of myocardial sections after HE staining for each group is shown in Fig. 2C. The model group exhibited distinct evidence of ischemic and necrotic tissues at the infarct end. The SNT group demonstrated reduced infarction extent and increased formation of new capillaries. Serum biochemical analysis revealed significantly elevated LDH, AST, and ALT levels in the model group, which notably decreased following SNT administration (Fig. 2D). These findings collectively confirmed the myocardial cell-protective effects of SNT, indicating its therapeutic potential for both acute and chronic myocardial infarction.

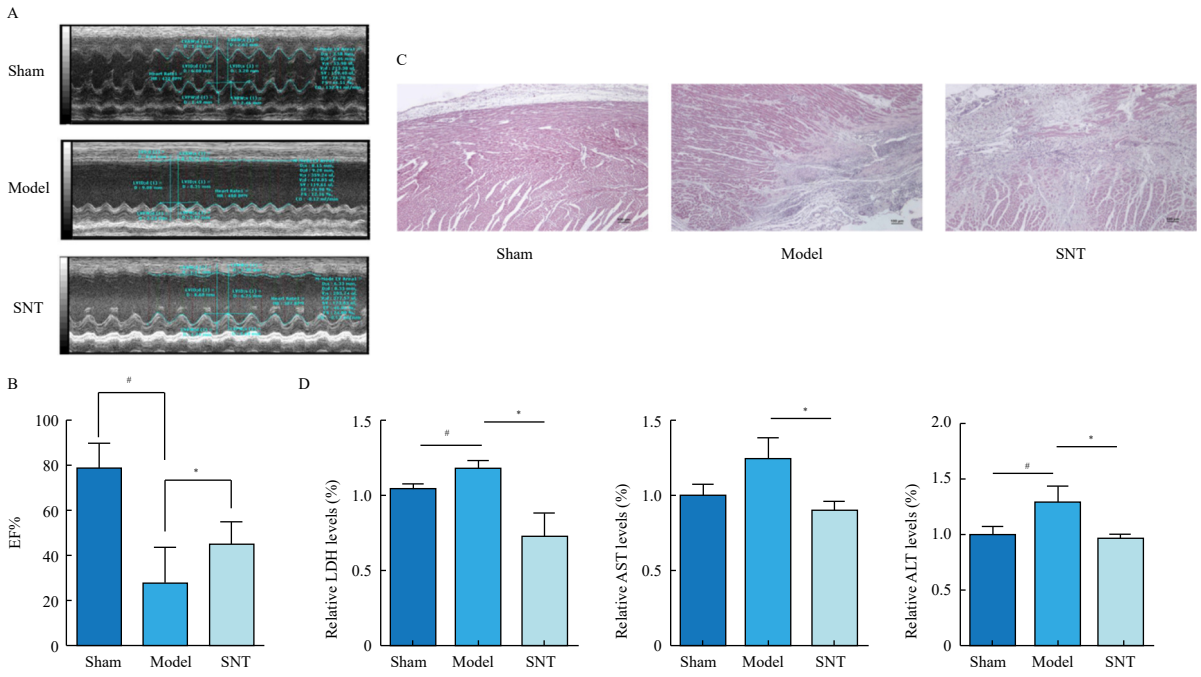

Fig. 2 The impact of SNT on the rat myocardial infarction model. (A) Typical echocardiography in Sham (n = 11), Model (n = 8), and SNT (n = 9) groups. The M-curve was drawn based on the average of 5 cardiac cycles. (B) EF% were analyzed by t-test. (C) The HE staining of rat myocardial tissue. (D) The effect of SNT on the levels of serum LDH, AST, and ALT in mice. Results represent means ± SD (n = 3), $^{\#}P < 0.05$, Sham *vs* Model; $^{*}P < 0.05$, SNT *vs* Model.

3.2. Label-free proteomic analysis

3.2.1. Quality control of protein sample

The system's reproducibility was evaluated by selecting No. 6 from the Sham group. The sample underwent nano LC-LTQ-Orbitrap MS analysis six times to assess variations in primary peak retention times. As illustrated in Fig. S1, the retention time variations of the main peptide segments' peaks across the six generated maps showed deviations below 2 min. This consistency level meets the requirements for label-free proteomics.

Fig. S2 presents the representative nano LC-LTQ-Orbitrap MS profiles for the three sample sets. The distribution of peptide ion retention times is shown in Fig. S3. The label-free proteomic analysis demonstrated that substantial peptide information could be obtained using a 50 cm-long column. The peptide molecular weight distribution displayed a clear pattern, with smaller segments eluting earlier than longer segments. This methodology proves effective for quantitative proteomic analysis.

Further analysis of peptide correlations across groups is shown in Fig. S4. The correlation coefficients (R^2) achieved values of 0.92 in the Sham group, 0.82 in the Model group, and 0.95 in the SNT group. These results indicate strong similarity among samples within each group, with minimal impact from inherent inter-animal variations or systemic errors. In contrast, the correlation between the Model and Sham groups was 0.76, while the correlation between the Model and SNT groups was 0.8. This indicates varying correlation strengths within the same peptide segment across different treatment groups. These findings warrant a detailed investigation of potential protein biomarkers.

3.3. Screening and functional analysis of differential protein

Protein identification and quantification were performed using MaxQuant 2.0.1.0. Following the criterion of identifying proteins with at least one uniquely matched peptide, 590 proteins were identified. As shown in Fig. 3A, 517 proteins were detected across all three groups, representing an 87.5% overlap. This in-

vestigation focused on analyzing the expression patterns of these 517 proteins within the three groups. Additionally, particular attention was given to examining the relevant information regarding the six proteins unique to the SNT treatment group.

To identify differentially expressed proteins, a significance threshold was established requiring fold changes ≥ 1.5-fold or ≤ 0.6-fold with a *P*-value of ≤ 0.05. The comparison between Sham and Model groups, presented in Table S1, utilized one-way ANOVA analysis. This analysis identified 30 significantly up-regulated proteins and 51 significantly down-regulated proteins. The distinct protein information was analyzed using the STRING database for Gene Ontology (GO) functional analysis. The primary functional categorization of these proteins was based on cellular components and biological processes (Figs. 3B and 3C). These proteins were primarily localized in cellular compartments, including the actin cytoskeleton, actin filament bundle, and actin filament. Functionally, these proteins were involved in fatty acid catabolic processes, actin filament organization, fatty acid *β*-oxidation, monocarboxylic acid catabolic processes, and organic acid catabolic processes. Previous studies identified PDI as a cardiomyocyte survival factor in ischemic cardiomyopathy [19], FIB as a predictor in patients with myocardial infarction [20-22], and CX43 expression as affected by myocardial infarction [23, 24]. Based on label-free proteomics analysis, FIB α, HSP90 α/β, PDIA3 and CX43 from the differential proteins cluster were validated by Western blotting, as shown in Fig. 3D. The results demonstrated that FIB α, HSP90 α/β, and PDIA3 protein expression decreased after SNT treatment, consistent with proteomic analysis findings in both Model and SNT groups, validating the accuracy of the large-scale label-free proteomics study. Additionally, IHC results indicated significantly reduced FIB α, HSP90 α/β, PDIA3 proteins in the hearts of SNT-treated rats (Fig. 3E). These experiments suggest SNT effectively reduces FIB α, HSP90 α/β and PDIA3 protein expression to achieve therapeutic effects in myocardial injury.

3.4. Targets identification of SNT by DARTS technology

To identify SNT targets, H9c2 cardiomyocytes were exposed to SNT (at a total alkaloid concentration of 100 μmol·L^{-1}). As shown in Figs. 4A and 4B, the optimized bidirectional fluorescence electrophoresis effectively separated all protein spots. This experiment was conducted in triplicate, demonstrating reproducibility for 80% of the protein spots, confirming the experimental system's stability and suitability for DARTS analysis in direct target screening. In the merged image (Fig. 4C), yellow fluorescence indicates unchanged proteins across groups, green fluorescence indicates proteins with elevated content in the administration group, and red fluorescence indicates proteins with higher content in the control group.

Through subsequent intensity analysis, protein spots showing significant changes were identified. These spots were excised from the gel and underwent silver staining and decolorization, followed by mass spectrometry identification after in-gel enzymatic digestion. Eleven protein spots were successfully identified, with results detailed in Table 1.

PDI represents a multifunctional protein primarily located in the mammalian endoplasmic reticulum. PDIA3, also known as glucose-regulated protein 58 (GRP58) or endoplasmic reticulum protein 57 (ERP57), belongs to the PDI family. The DARTS experiment revealed SNT's significant protective effect on PDIA3 protein, suggesting its potential role as a crucial target for SNT in protecting myocardial cells from apoptosis.

Recent studies have demonstrated that SM22 functions as an actin-binding protein with proliferative capabilities [25] and serves as a marker for various tumors, particularly breast cancer [26]. During H9c2 cardiomyocyte differentiation, SM22 expression exhibits a significant decrease. This reduction plays a role in both cell proliferation and differentiation processes, specifically through maintaining direct spatial interactions with tissue actin and supporting cytoskeletal stability. These observations suggest that SNT's potential mechanism in myocardial tissue protection may involve cytoskeletal stabilization.

Both destrin and cofilin-1 function as essential cytosolic actin-depolymerizing factors (ADFs), supporting cell morphology, migration, embryogenesis, angiogenesis, organ development, and tumor metastasis through cytoskeletal regulation. Aldose reductase, a critical rate-limiting enzyme in the polyol pathway, converts blood glucose to sorbitol and is associated with various cardiovascular conditions involving oxidative stress, including myocardial ischemia and heart failure [27]. Triosephosphate iso-

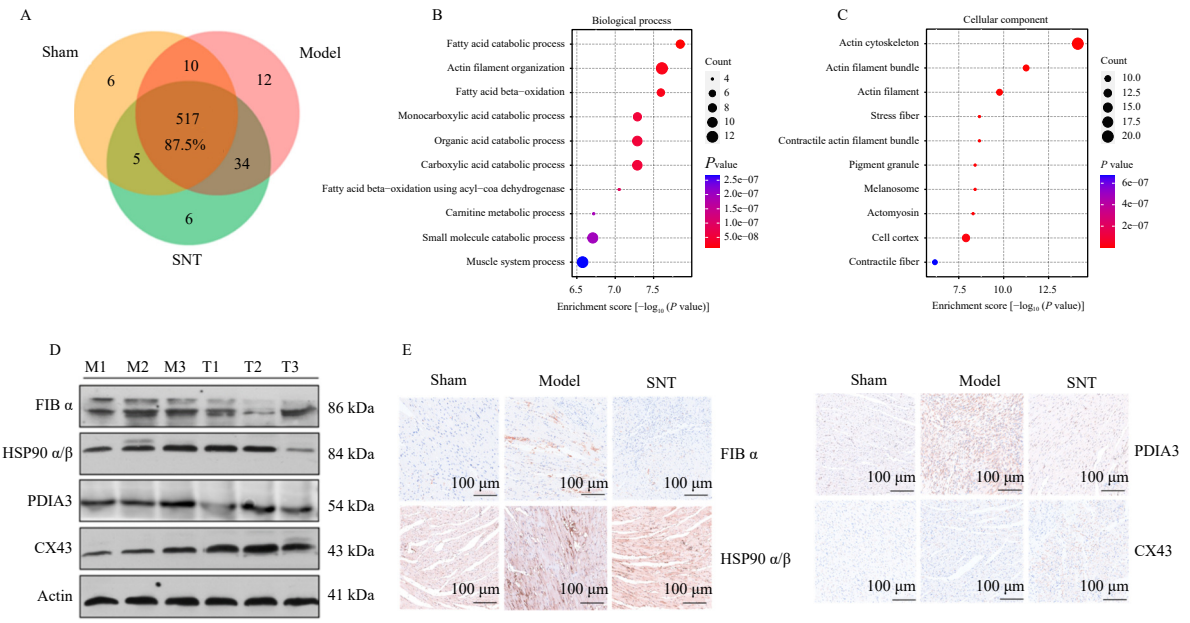

Fig. 3 Proteomic data analysis. (A)Protein sequence coverage among the three experimental groups as identified by LTQ-Orbitrap mass spectrometry. (B and C) GO classification of 81 differentially expressed proteins based on (B) cellular components and (C) biological processes. (D) Validation of differentially expressed proteins by Western blotting. FIB α, Fibrinogen α; CX43, gap junction alpha-1 protein; HSP90 α/β, heat shock protein 90 α/β; PDIA3, protein disulfide-isomerase A3; M: model group; T: SNT group. (E) Representative immunohistochemical staining of the above 4 proteins in left ventricular sections from Model and SNT groups (n = 3). Scale bar: 50 μm.

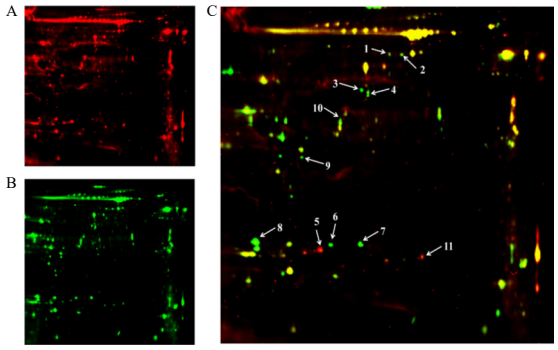

Fig. 4 The fluorescence result of differential proteins by DARTS-DIGE in the H9c2 cell line in (A) the Control group and (B) the SNT group (n = 3). (C)The merge plot of the Control and SNT groups in the DARTS-DIGE experiments. The green fluorescence spots indicate the higher contents in the SNT group, while the red fluorescence indicates the higher contents in the Control group.

merase catalyzes the reversible conversion between propanose phosphate isomers and plays an essential role in glycolysis and energy metabolism. Previous metabolomics studies suggest that SNT may exert its anti-heart failure and anti-myocardial infarction effects through the regulation of rat energy metabolism. Further research is needed to examine the decoction's effects on key metabolic pathway enzymes.

3.5. Network analysis and validation of potential target proteins

The differential protein results underwent functional and correlation analysis using the STRING protein functional classification database (http://www.string-db.org/). Protein-protein interaction results (Fig. 5A) revealed SNT's involvement in multiple processes: NADH biosynthesis, myocardial contraction promotion, cell morphology preservation, collagen synthesis contribution, aldolase activity, energy transport and metabolism, citric acid synthesis, 3-hydroxyisobutyl coenzyme A synthetase, and acetyl coenzyme A dehydrogenase. These functions collectively support myocardial cell protection and indicate potential applications in myocardial infarction treatment through ion channel activity modulation.

Additionally, we utilized the DOX-induced myocardial injury in H9c2 cells to assess SNT's effect on biological pathways and key genes or proteins. Phenotype and CCK-8 results demonstrate that SNT facilitates damaged cardiomyocyte recovery (Figs. 5B and 5C). Moreover, qPCR results showed that *Pdia3* mRNA expression decreased in SNT-treated myocardial injury cells, correlating with *Tpm2* expression (Fig. 5D). Furthermore, proteins involved in ERP processing, including Mogs, Lman2, and Mana1, exhibited downregulation after SNT treatment. These findings suggest that SNT provides myocardial injury protection through *Pdia3* modulation.

To investigate the cardioprotective effects of specific bioactive components from SNT against DOX-induced myocardial injury, Hig and Mes were selected for further validation in H9c2 cardiomyocytes. Cell viability assays using CCK-8 revealed that both Hig and Mes significantly improved cell survival compared to the DOX-treated group (Figs. 6A and 6B). Additionally, qPCR analysis demonstrated that both compounds attenuated the DOX-induced upregulation of *Pdia3* (Figs. 6C and 6D). Molecular docking analysis indicated effective binding of Hig and Mes to *Pdia3*, with binding affinities of −7.4 and −6.4 kcal·mol^{-1}, respectively. Hig demonstrated the strongest interaction, forming hydrogen bonds with residues Tyr-455, Ser-454, and Asp-451 (Figs. 6E and 6F). These findings establish a foundation for future *in vitro* and *in vivo* studies investigating these compounds' therapeutic potential in myocardial injury treatment.

PDIA3 engages in interactions with multiple proteins, including calreticulin (CALR), HSP90, endoplasmin (GRP94), PDIA1, and GRP78 [28, 29]. These proteins constitute an intricate network within the cell that regulates protein folding, assembly, and modification, thereby influencing cellular function and viability. The protein-protein interaction (PPI) analysis revealed two novel interaction proteins of PDIA3: β-tropomyosin (TPM2) and acyl-CoA synthetase long chain family member 1 (ACSL1). TPM2 serves as a primary component of muscle tissue, particularly in skeletal and cardiac muscle, while ACSL1 participates in the fatty acid metabolism pathway. PDIA3, along with its potential interacting proteins TPM2 and ACSL1, represent potential direct or indirect targets for myocardial targeting by SNT. This interaction maintains cellular homeostasis and prevents misfolded protein accumulation, which could otherwise lead to cellular dysfunction. Additional validation and comprehensive analysis are necessary to substantiate these findings.

Table 1 The differential expressed protein identified in DARTS-DIGE experiments.

Protein accession	Protein name	Unique peptide	Sequence coverage
P11598	Protein disulfide-isomerase A3	3	17%
P60711	Actin, cytoplasmic 1	3	20%
P62738	Actin, aortic smooth muscle	3	33%
P31232	Transgelin	4	35%
Q7M0E3	Destrin	4	27%
P45592	Cofilin-1	4	29%
P47727	Carbonyl reductase [NADPH] 1-like	5	35%
G3V786	Aldose reductase-related protein 1-like	5	24%
P48500	Triosephosphate isomerase	4	12%
Q68FR6	Elongation factor 1-gamma	4	12%
P63259	Actin, cytoplasmic 2	5	26%

4. Discussion

In summary, label-free proteomics technology identified 590 proteins in rat tissue samples, with 30 proteins significantly up-regulated and 51 proteins significantly down-regulated when comparing SNT with the Model group, using a critical threshold of fold change ≥ 1.5 & $P \leq 0.05$. Subsequently, DARTS-DIGE technology identified 11 differential proteins as direct targets of SNT treatment in H9c2 cell myocardia. As a protein biomarker and potential target, PDIA3 functions as an enzyme catalyzing intracellular intramolecular or intermolecular isomerization [30]. Evidence demonstrates that elevated PDI expression in cardiac myocytes provides protection against myocardial hypoxia-induced apoptosis. This protein plays a crucial role in ischemic or failing cardiac myocyte survival, thus maintaining myocardial physiological function [31-35]. Additionally, the identification and development of novel small-molecule PDI inhibitors have initiated a new phase of bench-to-bedside research.

All differentially expressed proteins were submitted to the STRING database (STRING: functional protein association networks; https://string-db.org) to establish PPI networks explore functional associations relevant to myocardial protection. Network analysis revealed clusters of proteins implicated in cardiac structure and metabolism, including myosin-related proteins, ion channel receptors, ATP synthase subunits, sarcoplasmic reticulum calcium ATPase 2, FIB α protein, gap junction α-1, HSP90, and NADH-related enzymes. Additionally, a subset of proteins, PDIA3, gliotransferrin, destrin, cofilin-1, aldose reductase, and phosphopropylglucose isomerase, were identified as putative dir-

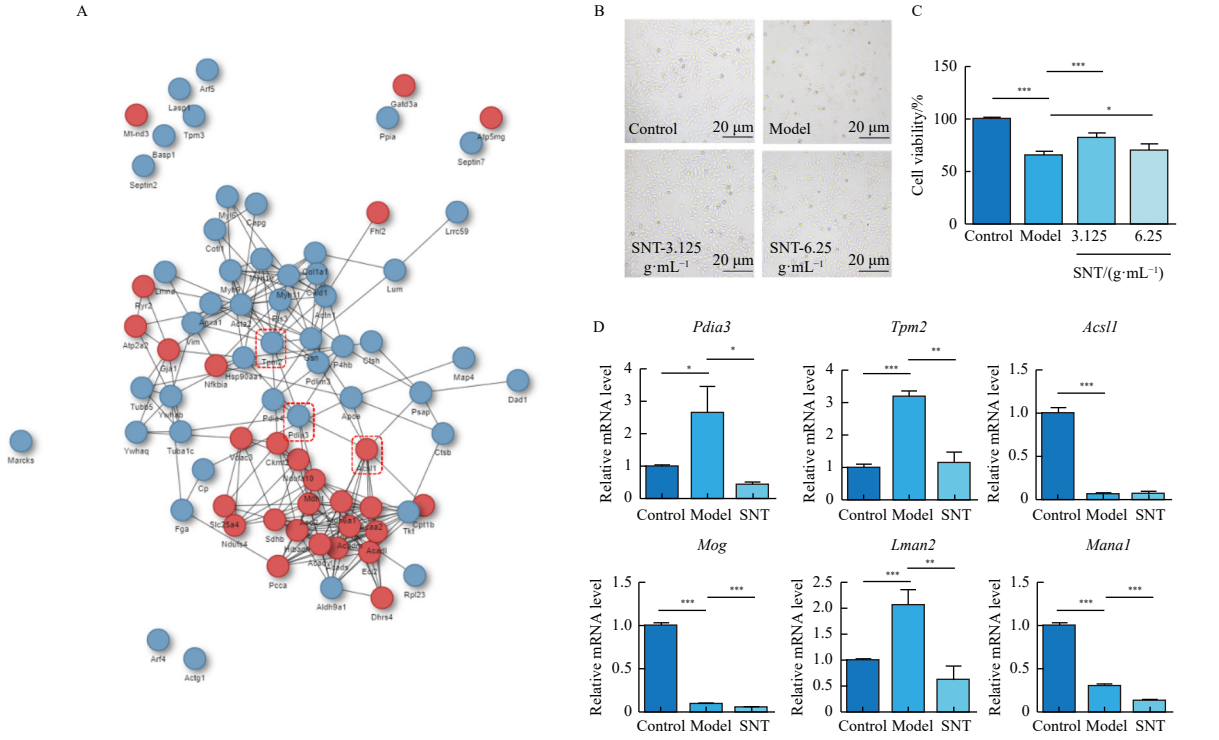

Fig. 5 The involved pathway and key proteins or genes effected by SNT on DOX-induced myocardial injury model. (A) The network analysis of the potential target proteins (confidence score ≥ 0.4). Blue dots represent down-regulation, and red dots represent up-regulation. (B) The phenotype of SNT on DOX-induced myocardial injury in H9c2 cells. (C) Cell viability measurement. (D) The expression analysis of related genes affected by SNT (3.25 g·mL^{-1}) on DOX-induced myocardial injury in H9c2 cells. Data are presented as mean ± SD (n = 3). $^{*}P < 0.05$, $^{**}P < 0.01$, $^{***}P < 0.001$.

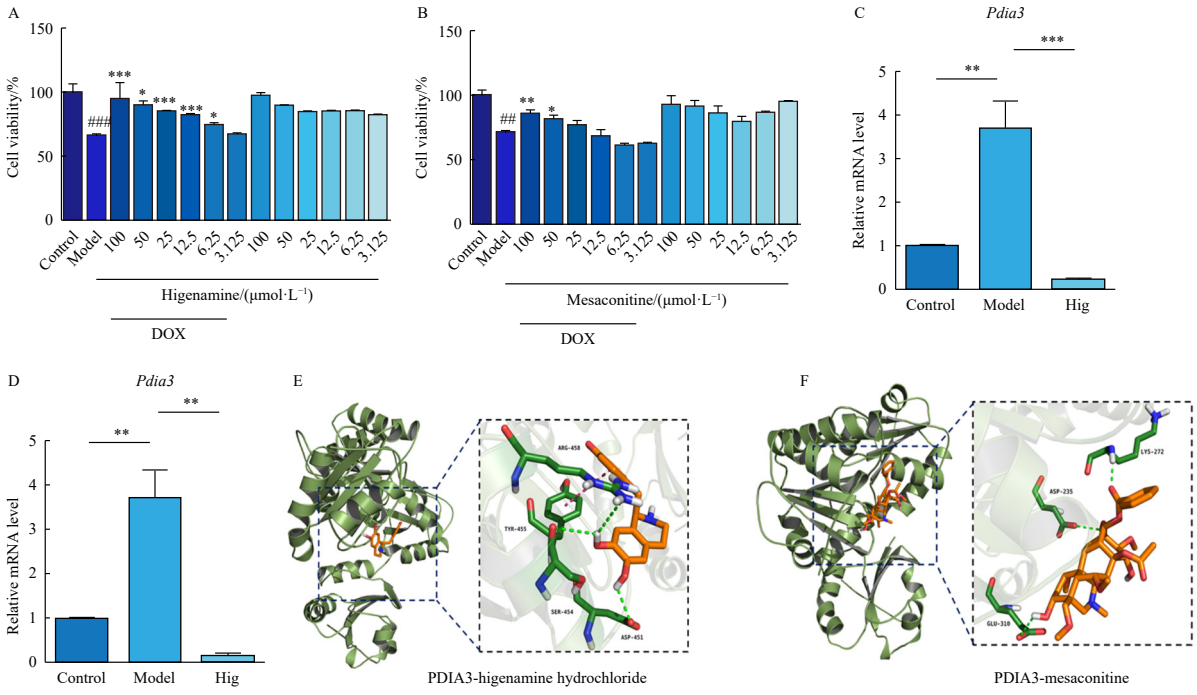

Fig. 6 The pharmacological effects of Hig and Mes selected from SNT on DOX-induced myocardial injury in H9c2 cells. (A and B) CCK8 analysis of Hig and Mes on DOX-induced myocardial injury in H9c2 cell. (C and D) The gene expression profile of *Pdia3* influenced by Hig and Mes on DOX-induced myocardial injury in H9c2 cells. Data are presented as mean ± SD (n = 3). $^{\#\#}P < 0.01$, $^{\#\#\#}P < 0.001$, Model group *vs* Control group; $^{*}P < 0.01$, $^{**}P < 0.01$, $^{***}P < 0.001$, Drug group *vs* Model group. (E and F) Docking analysis of PDIA3 (PDB: 7QNG) with its ligand Hig and Mes.

ect targets of SNT treatment based on their expression profiles and central positions within the network. Functional validation using CCK-8 assays and qPCR confirmed that PDIA3 and related proteins were significantly modulated by two bioactive compounds isolated from SNT, as well as by the complete SNT formulation, in a doxorubicin-induced myocardial injury model. Further studies, particularly *in vivo* and mechanistic investigations, are necessary to confirm the roles of these targets in mediating the therapeutic effects of SNT.

Proteomics encompasses techniques for identifying and

quantifying the complete protein content of a cell, tissue, or organism. It complements other "histological" techniques, including genomics and transcriptomics, to determine protein identity and elucidate specific protein structure and function [36]. The past decade has witnessed the development of various mass spectrometry-based proteomics methods that enable the study of protein conformational properties and protein-ligand complexes in complex biological mixtures, from cell lysates to intact cells [37]. These methodologies include chemical cross-linking (XL-MS), hydroxyl radical footprinting (HRF), DARTS, limited protein hydrolysis (LiP), pulsed PP, stability of proteins from oxidation rates (SPROX), and thermal proteomic analysis (TPP).

The DARTS method represents an innovative target discovery approach founded on LiP principles, initially developed for identifying small molecule protein targets. This method proves particularly effective for screening small molecule targets without requiring structural modifications [38-43]. Quantitative protein information is generated through bottom-up proteomics data obtained from LC-MS/MS analysis. Due to its straightforward implementation and high efficiency, the DARTS method has successfully elucidated drug mechanisms of action [44-47]. Furthermore, integrating DARTS with advancing MS technologies or comprehensive chemical proteomics expands its potential applications, enhancing its utility and appeal.

Funding

This work was supported by the National Natural Science Foundation of China (Nos. 82073814, 82122066, and 82104328), the "Dawn" Program of the Shanghai Education Commission (No. 22SG34), the National Key Research and Development Program of the Ministry of China (No. 2022YFC2704603), and Shanghai Sailing Program (No. 20YF1458900).

Availability of supporting information

Supporting information for this work can be obtained by contacting the corresponding authors *via* E-mail.

Declaration of competing interest

These authors have no conflict of interest to declare.

References

1 Tan G, Zhu Z, Jing J, et al. Characterization of constituents in Sini Decoction and rat plasma by high-performance liquid chromatography with diode array detection coupled to time-of-flight mass spectrometry. *Biomed Chromatogr*. 2011;25(8):913-924. https://doi.org/10.1002/bmc.1544.
2 Chen J, Ding Z. Advances in natural product anti-coronavirus research (2002–2022). *Chin Med*. 2023;18(1):13. https://doi.org/10.1186/s13020-023-00715-x.
3 Li Y, Lu Y, Nian M, et al. Therapeutic potential and mechanism of Chinese herbal medicines in treating fibrotic liver disease. *Chin J Nat Med*. 2023;21(9):643-657. https://doi.org/10.1016/S1875-5364(23)60443-1.
4 Wang SM, Ye LF, Wang LH. Traditional Chinese medicine enhances myocardial metabolism during heart failure. *Biomed Pharmacother*. 2022;146:112538. https://doi.org/10.1016/j.biopha.2021.112538.
5 Shu Z, Wu T, Shahen M, et al. System-pharmacology dissection of traditional Chinese herbs Sini Decoction for treatment of cardiovascular diseases. *An Acad Bras Cienc*. 2019;91(3):e20180424. https://doi.org/10.1590/0001-3765201920180424.
6 Zhang Z, Chen F, Wan J, et al. Potential traditional Chinese medicines with anti-inflammation in the prevention of heart failure following myocardial infarction. *Chin Med*. 2023;18(1):28. https://doi.org/10.1186/s13020-023-00732-w.
7 Sun S, Chen Q, Ge J, et al. Pharmacokinetic interaction of aconitine, liquiritin and 6-gingerol in a traditional Chinese herbal formula, Sini Decoction. *Xenobiotica*. 2018;48(1):45-52. https://doi.org/10.1080/00498254.2017.1278807.
8 Ding X, Zhang Y, Pan P, et al. Multiple mitochondria-targeted components screened from Sini Decoction improved cardiac energetics and mitochondrial dysfunction to attenuate doxorubicin-induced cardiomyopathy. *Theranostics*. 2023;13(2):510-530. https://doi.org/10.7150/thno.80066.
9 Tan G, Zhu Z, Zhang H, et al. Analysis of phenolic and triterpenoid compounds in licorice and rat plasma by high-performance liquid chromatography diode-array detection, time-of-flight mass spectrometry and quadrupole ion trap mass spectrometry. *Rapid Commun Mass Spectrom*. 2010;24(2):209-218. https://doi.org/10.1002/rcm.4373.
10 Gu Y, Fan F, Liu Y, et al. Cell-free protein synthesis system for bioanalysis: advances in methods and applications. *Trends Analyt Chem*. 2023;161:117015. https://doi.org/10.1016/j.trac.2023.117015.
11 Gu Y, Wang R, Chen P, et al. *In situ* synthesis and unidirectional insertion of membrane proteins in liposome-immobilized silica stationary phase for rapid preparation of microaffinity chromatography. *Acta Pharm Sin B*. 2022;12(9):3682-3693. https://doi.org/10.1016/j.apsb.2022.04.010.
12 Chai X, Gu Y, Lv L, et al. Screening of immune cell activators from Astragali Radix using a comprehensive two-dimensional NK-92MI cell membrane chromatography/C_{18} column/time-of-flight mass spectrometry system. *J Pharm Anal*. 2022;12(5):725-732. https://doi.org/10.1016/j.jpha.2022.05.006.
13 Chen X, Cao Y, Zhang H, et al. Comparative normal/failing rat myocardium cell membrane chromatographic analysis system for screening specific components that counteract doxorubicin-induced heart failure from *Acontium carmichaeli*. *Anal Chem*. 2014;86(10):4748-4757. https://doi.org/10.1021/ac500287e.
14 Chen S, Wu S, Li W, et al. Investigation of the therapeutic effectiveness of active components in Sini Decoction by a comprehensive GC/LC-MS based metabolomics and network pharmacology approaches. *Mol Biosyst*. 2014;10(12):3310-3321. https://doi.org/10.1039/C4MB00048J.
15 Feng F, Zhang W, Chai Y, et al. Label-free target protein characterization for small molecule drugs: recent advances in methods and applications. *J Pharm Biomed Anal*. 2023;223:115107. https://doi.org/10.1016/j.jpba.2022.115107.
16 Xia D, Liu B, Xu X, et al. Drug target discovery by magnetic nanoparticles coupled mass spectrometry. *J Pharm Anal*. 2021;11(1):122-127. https://doi.org/10.1016/j.jpha.2020.02.002.
17 Hwang HY, Kim TY, Szász MA, et al. Profiling the protein targets of unmodified bio-active molecules with drug affinity responsive target stability and liquid chromatography/tandem mass spectrometry. *Proteomics*. 2020;20(9):e1900325. https://doi.org/10.1002/pmic.201900325.
18 Chen S, Jiang H, Cao Y, et al. Drug target identification using network analysis: taking active components in Sini Decoction as an example. *Sci Rep*. 2016;6:24245. https://doi.org/10.1038/srep24245.
19 Severino A, Campioni M, Straino S, et al. Identification of protein disulfide isomerase as a cardiomyocyte survival factor in ischemic cardiomyopathy. *J Am Coll Cardiol*. 2007;50(11):1029-1037. https://doi.org/10.1016/j.jacc.2007.06.006.
20 Jia C, Wu W, Lu H, et al. Fibrinogen to HDL-cholesterol ratio as a predictor of mortality risk in patients with acute myocardial infarction. *Lipids Health Dis*. 2024;23(1):86. https://doi.org/10.1186/s12944-024-02071-7.
21 Mannila MN, Lovely RS, Kazmierczak SC, et al. Elevated plasma fibrinogen γ concentration is associated with myocardial infarction: effects of variation in fibrinogen genes and environmental factors. *J Thromb Haemost*. 2007;5(4):766-773. https://doi.org/10.1111/j.1538-7836.2007.02406.x.
22 Mjelva ØR, Svingen GFT, Pedersen EKR, et al. Fibrinogen and neopterin is associated with future myocardial infarction and total mortality in patients with stable coronary artery disease. *Thromb Haemost*. 2018;118(4):778-790. https://doi.org/10.1055/s-0038-1629912.
23 Ke J, Zhu C, Zhang Y, et al. Anti-arrhythmic effects of linalool *via* Cx43 expression in a rat model of myocardial infarction. *Front Pharmacol*. 2020;11:926. https://doi.org/10.3389/fphar.2020.00926.
24 Martins-Marques T, Ribeiro-Rodrigues T, de Jager SC, et al. Myocardial infarction affects Cx43 content of extracellular vesicles secreted by cardiomyocytes. *Life Sci Alliance*. 2020;3(12):e202000821. https://doi.org/10.26508/lsa.202000821.
25 Assinder SJ, Stanton JA, Prasad PD. Transgelin: an actin-binding protein and tumour suppressor. *Int J Biochem Cell Biol*. 2009;41(3):482-486. https://doi.org/10.1016/j.biocel.2008.02.011.
26 Sahasrabuddhe NA, Barbhuiya MA, Bhunia S, et al. Identification of prosaposin and transgelin as potential biomarkers for gallbladder cancer using quantitative proteomics. *Biochem Biophys Res Commun*. 2014;446(4):863-869. https://doi.org/10.1016/j.bbrc.2014.03.017.
27 Son NH, Ananthakrishnan R, Yu S, et al. Cardiomyocyte aldose reductase causes heart failure and impairs recovery from ischemia. *PLoS One*. 2012;7(9):e46549. https://doi.org/10.1371/journal.pone.0046549.
28 Wang K, Li H, Chen R, et al. Combination of CALR and PDIA3 is a potential prognostic biomarker for non-small cell lung cancer. *Oncotarget*. 2017;8(57):96945-96957. https://doi.org/10.18632/oncotarget.18547.
29 Chichiarelli S, Altieri F, Paglia G, et al. ERp57/PDIA3: new insight. *Cell Mol Biol Lett*. 2022;27(1):12. https://doi.org/10.1186/s11658-022-00315-x.
30 Sakai J, Ishikawa H, Kojima S, et al. Proteomic analysis of rat heart in ischemia and ischemia-reperfusion using fluorescence two-dimensional difference gel electrophoresis. *Proteomics*. 2003;3(7):1318-1324. https://doi.org/10.1002/pmic.200300432.
31 Tian F, Zhou X, Wikström J, et al. Protein disulfide isomerase increases in myocardial endothelial cells in mice exposed to chronic hypoxia: a stimulatory role in angiogenesis. *Am J Physiol Heart Circ Physiol*. 2009;297(3):H1078-H1086. https://doi.org/10.1152/ajpheart.00937.2008.
32 Toldo S, Boccellino M, Rinaldi B, et al. Altered oxido-reductive state in the diabetic heart: loss of cardioprotection due to protein disulfide isomerase. *Mol Med*. 2011;17(9-10):1012-1021. https://doi.org/10.2119/molmed.2011.00100.
33 Toldo S, Severino A, Abbate A, et al. The role of PDI as a survival factor in cardiomyocyte ischemia. *Methods Enzymol*. 2011;489:47-65. https://doi.org/10.1016/B978-0-12-385116-1.00003-0.
34 Xiong B, Jha V, Min JK, et al. Protein disulfide isomerase in cardiovascular

disease. *Exp Mol Med*. 2020;52(3):390-399. https://doi.org/10.1038/s12276-020-0401-5.
35 Cho J. Protein disulfide isomerase in thrombosis and vascular inflammation. *J Thromb Haemost*. 2013;11(12):2084-2091. https://doi.org/10.1111/jth.12413.
36 Aslam B, Basit M, Nisar MA, et al. Proteomics: technologies and their applications. *J Chromatogr Sci*. 2017;55(2):182-196. https://doi.org/10.1093/chromsci/bmw167.
37 Kaur U, Meng H, Lui F, et al. Proteome-wide structural biology: an emerging field for the structural analysis of proteins on the proteomic scale. *J Proteome Res*. 2018;17(11):3614-3627. https://doi.org/10.1021/acs.jproteome.8b00341.
38 Lomenick B, Hao R, Jonai N, et al. Target identification using drug affinity responsive target stability (DARTS). *Proc Natl Acad Sci U S A*. 2009;106(51):21984-21989. https://doi.org/10.1073/pnas.0910040106.
39 Lomenick B, Olsen RW, Huang J. Identification of direct protein targets of small molecules. *ACS Chem Biol*. 2011;6(1):34-46. https://doi.org/10.1021/cb100294v.
40 Gong F, Peng X, Sang Y, et al. Dichloroacetate induces protective autophagy in LoVo cells: involvement of cathepsin D/thioredoxin-like protein 1 and Akt-mTOR-mediated signaling. *Cell Death Dis*. 2013;4(11):e913. https://doi.org/10.1038/cddis.2013.438.
41 Pai MY, Lomenick B, Hwang H, et al. Drug affinity responsive target stability (DARTS) for small-molecule target identification. *Methods Mol Biol*. 2015;1263:287-298. https://doi.org/10.1007/978-1-4939-2269-7_22.
42 Dal Piaz F, Vera Saltos MB, Franceschelli S, et al. Drug affinity responsive target stability (DARTS) identifies laurifolioside as a new clathrin heavy chain modulator. *J Nat Prod*. 2016;79(10):2681-2692. https://doi.org/10.1021/acs.jnatprod.6b00627.
43 Ren YS, Li HL, Piao XH, et al. Drug affinity responsive target stability (DARTS) accelerated small molecules target discovery: principles and application. *Biochem Pharmacol*. 2021;194:114798. https://doi.org/10.1016/j.bcp.2021.114798.
44 Kim D, Hwang HY, Kim JY, et al. FK506, an immunosuppressive drug, induces autophagy by binding to the V-ATPase catalytic subunit A in neuronal cells. *J Proteome Res*. 2017;16(1):55-64. https://doi.org/10.1021/acs.jproteome.6b00638.
45 Gotsbacher MP, Cho SM, Kim NH, et al. Reverse chemical proteomics identifies an unanticipated human target of the antimalarial artesunate. *ACS Chem Biol*. 2019;14(4):636-643. https://doi.org/10.1021/acschembio.8b01004.
46 Cho SM, Lee HK, Liu Q, et al. A guanidine-based synthetic compound suppresses angiogenesis *via* inhibition of acid ceramidase. *ACS Chem Biol*. 2019;14(1):11-19. https://doi.org/10.1021/acschembio.8b00558.
47 Jia D, Liu C, Zhu Z, et al. Novel transketolase inhibitor oroxylin A suppresses the non-oxidative pentose phosphate pathway and hepatocellular carcinoma tumour growth in mice and patient-derived organoids. *Clin Transl Med*. 2022;12(11):e1095. https://doi.org/10.1002/ctm2.1095.